J Comput Aided Mol Des (2012) 26:215–232
DOI 10.1007/s10822-012-9550-5

Energetic basis for drug resistance of HIV-1 protease mutants against amprenavir

Parimal Kar · Volker Knecht

Received: 28 June 2011 / Accepted: 31 January 2012 / Published online: 14 February 2012

Abstract Amprenavir (APV) is a high affinity (0.15 nM) HIV-1 protease (PR) inhibitor. However, the affinities of the drug resistant protease variants V32I, I50V, I54V, I54M, I84V and L90M to amprenavir are decreased 3 to 30-fold compared to the wild-type. In this work, the popular molecular mechanics Poisson-Boltzmann surface area method has been used to investigate the effectiveness of amprenavir against the wild-type and these mutated protease variants. Our results reveal that the protonation state of Asp25/Asp25′ strongly affects the dynamics, the overall affinity and the interactions of the inhibitor with individual residues. We emphasize that, in contrast to what is often assumed, the protonation state may not be inferred from the affinities but requires pK_a calculations. At neutral pH, Asp25 and Asp25′ are ionized or protonated, respectively, as suggested from pK_a calculations. This protonation state was thus mainly considered in our study. Mutation induced changes in binding affinities are in agreement with the experimental findings. The decomposition of the binding free energy reveals the mechanisms underlying binding and drug resistance. Drug resistance arises from an increase in the energetic contribution from the van der Waals interactions between APV and PR (V32I, I50V, and I84V mutant) or a rise in the energetic contribution from the electrostatic interactions between the inhibitor and its target (I54M and I54V mutant). For the V32I mutant, also an increased free energy for the polar solvation contributes to the drug resistance. For the L90M mutant, a rise in the van der Waals energy for APV-PR interactions is compensated by a decrease in the polar solvation free energy such that the net binding affinity remains unchanged. Detailed understanding of the molecular forces governing binding and drug resistance might assist in the design of new inhibitors against HIV-1 PR variants that are resistant against current drugs.

Keywords HIV-1 PR · Drug resistance · Amprenavir · MM-PBSA · Normal mode analysis

Introduction

According to the UNAIDS 2009 report (http://www.unaids.org), ~60 million people world wide have been infected with the acquired immune deficiency syndrome (AIDS) with 25 million deaths. AIDS is caused by the human immunodeficiency virus (HIV). The World Health Organization (WHO) has declared AIDS as a pandemic. HIV type 1 protease (HIV-1 PR) is responsible for the cleavage of the viral *gag* and *pol* polyproteins into mature, functional proteins. Since inhibition of the HIV-1 PR activity prevents the maturation of these viral proteins, and thus the replication of the virus, HIV-1 PR has been an important target for anti-AIDS drug therapy.

The HIV-1 PR is a homodimeric aspartic protease composed of residues 1–99 and 1′–9′ (see Fig. 1). Each monomer comprises an α-helix and two anti-parallel β-sheets. The active site is evolutionary conserved and

Electronic supplementary material The online version of this article (doi:10.1007/s10822-012-9550-5) contains supplementary material, which is available to authorized users.

P. Kar · V. Knecht (✉)
Department of Theory and Bio-Systems, Max Planck Institute of Colloids and Interfaces, Am Mühlenberg 1, 14476 Potsdam, Germany
e-mail: Volker.Knecht@mpikg.mpg.de

P. Kar
e-mail: Parimal.Kar@mpikg.mpg.de

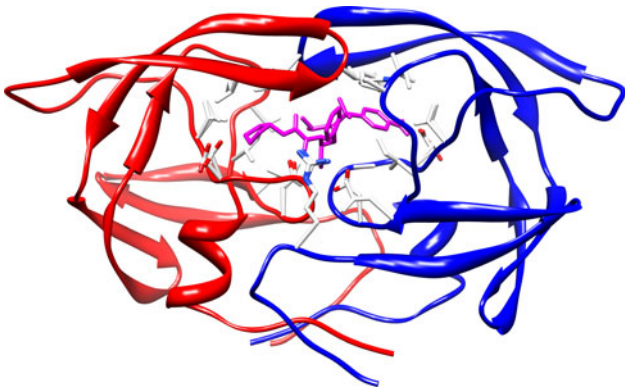

Fig. 1 Wild-type HIV-1 PR dimer with bound drug amprenavir (*magenta*). Each monomer is shown with a distinct color

composed of the conserved catalytic triad, Asp25(25′)–Thr26(26′)–Gly27(27′). The Asp dyad, Asp25 and Asp25′, constitutes the active site base; it is planar and interacts directly with substrates and inhibitors. Mutational analysis by several groups of the highly conserved Asp25 has shown that substituting this residue with Asn [1], Thr [2], or Ala [3] leads to a protein without any proteolytic activity.

The enzyme active site is gated by two extended β hairpin loops (residues 46–56), known as the flap regions, which presumably open and close to allow entry and binding of drugs [4, 5]. Three characteristic regions are observed in the flaps. The first region is composed of Met46–Phe53–Lys55 whose side chains extended toward the solvent. On the other hand, the second region contains Ile47–Ile54–Ile56 whose hydrophobic chains point inward. The third region is glycine-rich and made up of Gly48–Gly49–Gly51–Gly52. Together with Ile50, this third region forms the highly flexible flap tip at the head of the flaps.

With the introduction of highly active antiretroviral drugs, the treatment of HIV/AIDS patients has been improved, effectively decreasing the mortality rate of HIV/AIDS patients [6]. Developing vaccines to fight the AIDS infection is challenging [7]. Nine protease inhibitors have been approved by the Food and Drug Administration (FDA) for HIV therapy. These drugs are saquinavir (SQV), ritonavir (RTV), indinavir (IDV), nelfinavir (NFV), amprenavir (APV), lopinavir (LPV), atazanavir (AZV), tipranavir (TPV), and darunavir (DRV). However, the effectiveness of these inhibitors are limited by the occurrence of drug resistant mutations in the target enzyme caused by the high replication rate of HIV-1 and lack of a proof-reading mechanism in its reverse transcriptase (RT) [8]. To date, over 50 different drug resistance mutations at almost 30 different codon positions of HIV-1 PR have been characterized [9], mainly arising due to the gene's highly polymorphic nature. Even in the absence of anti-retroviral drugs HIV is genetically

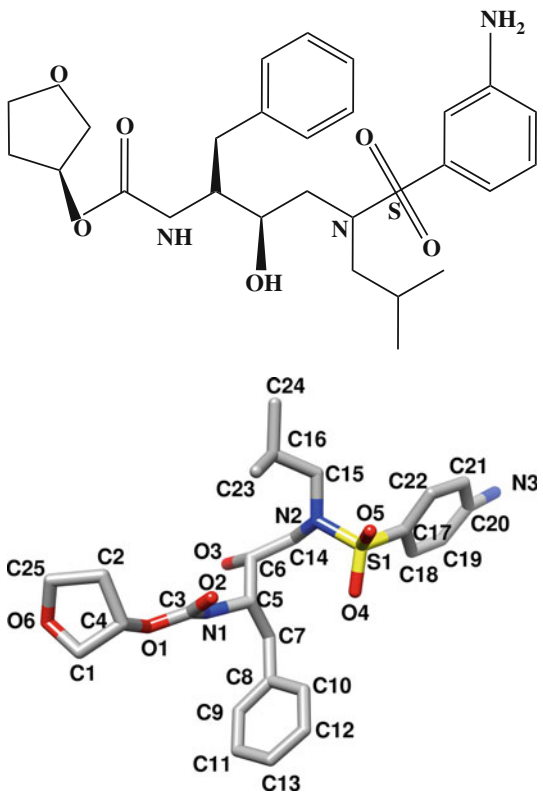

Fig. 2 Chemical structure of APV (*top*). Same structure in stick representation with atom number (*bottom*), here the colors distinguish between carbon (*gray*), oxygen (*red*), nitrogen (*blue*), and sulfur (*yellow*)

diverse, especially in the protease gene that showed variations in up to 50 different residues [10].

In this work, we have studied the binding of the protease inhibitor (PI) amprenavir (APV) with the wild-type protease and mutant variants. Amprenavir is the first protease inhibitor which includes a sulfonamide group. It was approved by the Food and Drug Administration in the year 1999. The chemical structure of amprenavir is shown in Fig. 2. Amprenavir was designed to maximize the hydrophobic interactions with the protease. The sulfonamide group increases the water solubility of amprenavir (60 μg mL^{-1}) [11]. The transition state of the enzyme is mimicked by the hydroxyethylamine core of amprenavir [11]. These core elements act as noncleavable peptide isosteres to mimic the transition state formed by the HIV-1 protease substrates during cleavage, thereby effectively inhibiting the enzyme. Basically, the core is a good isostere replacement at the scissile bond that is believed to mimic the tetrahedral transition state of the proteolytic reaction [12].

Of particular importance is the protonation state of the Asp dyad due to its direct contact with the substrate and the inhibitors. The Asp residues in the dyad can be either both unprotonated (unpro) or both protonated (dipro), or only Asp25 (mono25) or only Asp25′ could be protonated

(mono25′). The X-ray crystallographic structures do not contain hydrogen atoms and information about the protonation state can not be directly obtained from the X-ray data. NMR experiments yield different protonation states depending on the structure of the protease inhibitors; such experiments suggested HIV-1 PR to be in a monoprotonated state when bound to pepstatin [13] but in a deprotonated state when bound to inhibitors with diol groups [18].

Previous energetic analyses showed that the protonation state of the Asp dyad influences the dimerization of HIV-1 PR and the affinity of inhibitors for HIV-1 PR. Endpoint free energy calculations using the molecular mechanics Poisson-Boltzmann surface area (MM-PBSA) method show that the inhibitor BEA369 binds most strongly to HIV-1 PR in the mono25 state [14]. A study using free energy perturbation indicated that the HIV-1 PR in the mono25 state is also the protonation state with the highest affinity for the S and R isomer of the inhibitor U85548E [15]. The same protonation state also binds most strongly to saquinavir as indicated from a study using density functional theory, ONIOM, and MM-PBSA by Wittayanarakul et al. [16]. Recently Wittayanarakul et al. [17] have calculated binding free energies for the inhibitors lopinavir, ritonavir, saquinavir, indinavir, amprenavir, and nelfinavir bound to HIV-1 protease using the MM-PB(GB)SA method. They have considered all possible protonation states of the Asp25 dyad in their study. However, they have considered only the wild type protease. The binding free energy obtained from our calculations matches better with the experimental result compared to the binding free energy obtained by Wittayanarakul et al. In our calculations, all four possible protonation states of the Asp dyad were considered. If present, protons were attached to the OD2 atom of Asp25/Asp25′.

The HIV-1 resistance against protease inhibitors arises mainly due to the occurrence of mutations in the protease that significantly impair the protease's interaction with drugs but not with substrates. Mutations could occur at residues directly interacting with the inhibitors or far away from the inhibitor binding site [21]. These drug-resistant protease variants lose their high binding affinity to the inhibitors, while maintaining enough enzyme activity for the virus to propagate. Conservative mutations of hydrophobic residues are common in protease inhibitor resistance, including V32I, I50V, I54V, I54M, I84V, and L90M which are the focus of this study. The locations of these mutations in the protease dimer are shown in Fig. 3. The multi-drug resistant mutation V32I, which alters a residue in the active site cavity, appears in nearly 20% of patients treated with amprenavir [22] and is associated with a high level of drug resistance to lopanivir/ritonavir [23]. Wang and Kollman [24] proposed the following mechanism for the drug resistance: "if a residue is not conserved, presumably it is not important for viral function, but" if it "interacts more favorably with a drug than with the substrate, mutations of this residue may not affect the function of the protease but may impair the binding of the drug and thus cause resistance to the drug".

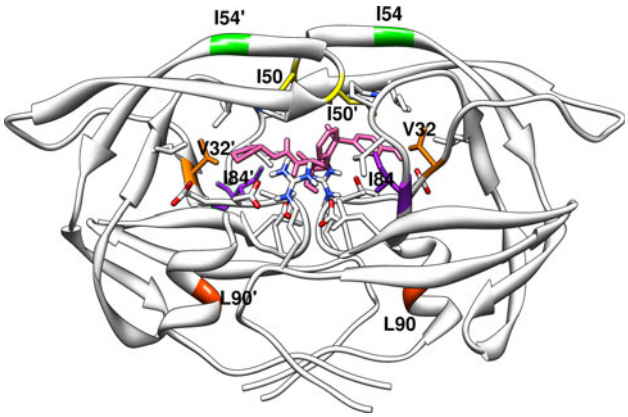

Fig. 3 Position of the mutations in the PR–APV complex. The position of each mutation is marked with different color. The APV is shown in *pink*

To understand the mechanism underlying the binding of wild-type protease and its mutant variants to amprenavir from an energetic point of view, we have used molecular dynamics simulations and free energy calculations to study the contributions to the binding affinities for the respective complexes. The most rigorous and accurate methods to calculate binding free energies are free energy perturbation (FEP) [25] and thermodynamic integration (TI) [26], however, these methods are computationally very expensive. In contrast, the MM-PBSA method [27–29] is faster by several orders of magnitude than FEP or TI. The MM-PBSA scheme is followed in our current study.

In MM-PBSA methods, the binding free energy is estimated as an average of molecular mechanical energies and solvation free energies of an ensemble of configurations of molecular complex obtained from a trajectory of a molecular dynamics simulation in explicit water. The MM-PB(GB)SA methods have successfully been used to estimate the binding free energy of protein-ligand [30, 31] and protein-RNA [32, 33] associations. These methods have also been used to study the binding of different inhibitors to protease [34–39] and reverse transcriptase (RT) [40]. Recently Worch et al. [41] have modeled the interaction propensity of the transmembrane domain (TMD) pairs and computed free energy gain resulting from TMD dimer formation using the MM-PBSA approach. In contrast to our approach, the PBSA term was replaced with the multiple continua approach established to mimic biomembrane environments: aqueous domain modeled by water, polar head group domain by ethanol, hydrophobic core domain modeled by cyclohexane [42].

Hou and Yu [39] studied the mechanism for binding and drug resistance for amprenavir in complex with the wild-type and V82F/I84V double mutant protease. On the other hand, we have studied the binding of amprenavir to wild-type and six single mutant variants. Hou and Yu predicted the binding free energy for the PR_{WT}–APV to be −20.02 kcal/mol while the experimental binding free energy was −13.4 kcal/mol. We have been able to predict the binding free energy close to the experimental value. They have used a short simulation (1.5 ns) in explicit water to generate an ensemble of configurations. In their study 160 configurations were used to estimate the binding free energy. Only 25 configurations were used by them to estimate the entropy. In contrast we have used 2,000 configurations for estimating the binding free energy, and the normal mode analysis was performed using 200 configurations.

The contribution from the change in entropy of the binding partners was obtained from a normal mode analysis of the complex and the individual binding partners. The results of our calculations agree well with experimental data [11] and give insights into the origins of mutation-induced affinity changes and, thus, the mechanism of drug-resistance.

Materials and methods

The free energies for the formation of HIV-1 PR–APV complexes were evaluated by simulating the corresponding complexes in explicit water and rescoring the free energies of the resulting configurations with an implicit solvent model.

Structure generation with periodic boundary MD simulations in explicit water

The initial coordinates for our simulations were obtained from the X-ray crystallographic structures of the HIV-1 PR complexed with the drug amprenavir (APV). Shen and coworkers [11] have determined the X-ray crystallographic structures of the wild-type HIV-1 PR and its mutant variants complexed with amprenavir at resolutions of 1.02–1.85 Å. The atomic coordinates with the Protein Data Bank accession code 3NU3 for wild-type HIV-1 PR–APV, 3NU4 for PR_{V32I}–APV, 3NU5 for PR_{I50V}–APV, 3NU6 for PR_{I54M}–APV, 3NUJ for PR_{I54V}–APV, 3NU9 for PR_{I84V}–APV and 3NUO for PR_{L90M}–APV were used for our current study. The structures 3NU3 and 3NU5 had the inhibitor bound in two conformations. Conformations with higher occupancy were selected for our simulations. All crystal water molecules in the crystal structure of the protease-amprenavir complexes were kept in the starting model. Four different types of protonations were assigned to Asp25/Asp25′. The proteins were described using the Amber ff99SB force field [43]. The ligand was assigned generalized amber force field (GAFF) [44] atom types, and AM1-BCC [45] atomic charges calculated with the *antechamber* [46] module of Amber [47]. Our previous work [48] shows that this charge scheme is suitable for this kind of study. The configurations were generated via simulations of the complexes in explicit water.

The complex was solvated in TIP3P [49] water using a truncated octahedron periodic box, extending at least 10 Å from the complex. Nearly 9,500 water molecules were added to solvate the complex and the resulting box size was nearly 90 × 90 × 90 Å. An appropriate number of chloride ions were added to neutralize the charge of the system. All bond lengths involving hydrogen atoms were constrained using the SHAKE [50] algorithm allowing the usage of a 2 fs time-step. The temperature was kept fixed at 300 K using a Langevin thermostat with a collision frequency of 2 ps^{-1}. The electrostatics were treated with the particle-mesh Ewald (PME) [51] scheme with a fourth-order B-spline interpolation and a tolerance of 10^{-5}. The non-bonded cut-off was 8 Å and the non-bonded pair list was updated every 50 fs.

The following protocol was used in our simulations: (a) the complex was first optimized by 500 steps of steepest descent followed by another 500 steps of conjugate gradient minimization, keeping all atoms of the complex restrained to their initial position with a weak harmonic restraint. (b) After the minimization, 50 ps of constant volume MD simulation with a 2 kcal mol^{-1} $Å^{-2}$ restraint on the complex was performed in order to equilibrate the solvent at 300 K without undesirable drifts of the structure. (c) Next, a 50 ps MD simulation with a 2 kcal mol^{-1} $Å^{-2}$ restraint on the complex was carried out at a pressure of 1 atm to equilibrate the density using Berendsen's barostat. (d) Then, the complex was equilibrated for 1 ns without restraint. After the equilibration phase, a 20 ns simulation at constant pressure was conducted and the coordinates were saved every 10 ps, resulting in 2,000 configurations for each simulation. Four sets of simulations with different protonation states of Asp25/Asp25′ were performed for each protease-inhibitor complex, considering the unpro, mono25, mono25′, and the dipro state of the Asp dyad.

MM-PBSA calculations

The protease-inhibitor (P–I) complex formation reaction is represented by the reaction scheme

$$[P]_{aq} + [I]_{aq} \longleftrightarrow [PI]_{aq} \quad (1)$$

where all the reactants are assumed to be in aqueous solution. The binding affinity is determined from the free

energies of the receptor/protease (P), the ligand/inhibitor (I), and the complex (PI) according to

$$\Delta G_{\text{bind}} = G_{\text{PI}} - (G_{\text{P}} + G_{\text{I}}) \quad (2)$$

The free energy of each species (P, I, PI) is estimated from

$$G = \langle E_{\text{MM}} \rangle + \langle G_{\text{pol}} \rangle + \langle G_{\text{np}} \rangle - T\langle S_{\text{MM}} \rangle. \quad (3)$$

Here, E_{MM} is the molecular mechanics gas-phase energy of the species, G_{pol} is the polar contribution to the solvation free energy of the species, estimated from the solution of the linear Poisson-Boltzmann (PB) equation, G_{np} is the non-polar solvation free energy, estimated from the solvent accessible surface area (SASA) of the species, T is the absolute temperature of the system, and S_{MM} is the entropy of the species. The gas-phase molecular mechanics energy E_{MM} can be expressed as

$$E_{\text{MM}} = E_{\text{cov}} + E_{\text{elec}} + E_{\text{vdW}}, \quad (4)$$

where E_{cov}, E_{elec}, and E_{vdW} denote the contributions from covalent, electrostatic, and van der Waals interactions, respectively. The entropic contributions to the binding free energies arising from changes in the translational (S_{trans}) degrees of freedom at a standard concentration of 1 M, as well as the rotational (S_{rot}) and vibrational (S_{vib}) degrees of freedom, are considered according to

$$S_{\text{MM}} = S_{\text{trans}} + S_{\text{rot}} + S_{\text{vib}}. \quad (5)$$

The nonpolar solvation term (G_{np}) was estimated from [52]

$$G_{\text{np}} = \gamma \text{A} + b \quad (6)$$

where γ is a surface tension parameter set to $\gamma = 0.00542$ kcal mol^{-1} Å^{-2} and b is a parameterized value set to $b = 0.92$ kcal.mol^{-1}. A is the solvent accessible surface area and was estimated using a probe radius of 1.4 Å with a fast Linear Combination of Pairwise Overlap (LCPO) [53] algorithm.

The averages in Eq. 3 are calculated from an ensemble of molecular configurations taken from a molecular dynamics simulation to capture the effects of motion. In order to mimic the in vitro binding event and to include the effects of the conformational changes upon binding, each of the three terms in Eq. 2 should be calculated from an individual simulation of the protein, the ligand and the complex, respectively (multi-trajectories method) [54]. As this scheme relies on sufficient sampling of configurational space, computational resources and time would be an issue. In practice, in order to reduce the time-consumption in simulation and to obtain stable energies, only the complex is simulated and all the three free energy terms are estimated from this single molecular dynamics trajectory [54, 55]. In that case, the covalent energy (E_{cov}) as well as the intramolecular electrostatic and van der Waals energy cancel out in the calculation of ΔG_{bind}. This single trajectory method is based on the assumption that conformational changes of the protein and ligand upon binding are negligible. Taking the structures of all the three species from a single trajectory may remove the noise resulting from sampling inconsistencies and reduce the inherent error in force field and implicit solvation energies. Nevertheless, earlier studies [54, 56] have shown that the multi-trajectory and the single trajectory method yield similar trends.

Explicit crystal water molecules were included in our free energy calculations. To this aim, explicit water molecules were considered as a part of the receptor. Thus, the binding free energy could be obtained from the following Eq. 7, which is standard MM-PBSA approach for including selected solvent molecules:

$$\Delta G_{\text{bind}} = \Delta G_{\text{PI+WAT}} - (\Delta G_{\text{P+WAT}} + \Delta G_{\text{I}}) \quad (7)$$

The total molecular-mechanical energy (E_{gas}), the covalent energy (E_{cov}), as well as the van der Waals (E_{vdW}), and electrostatic (E_{elec}) components were determined using the MMPBSA.py.MPI script in Amber-11. This script performs automatically all the required steps to estimate the binding free energy of protein-ligand complexes using the MM-PBSA method. The electrostatic contribution to the solvation free energy (G_{PB}) was estimated using the Poisson-Boltzmann (PB) approach using the *pbsa* solver implemented in Amber. In order to solve the PB equation, the grid spacing was set to 0.5 Å in all dimensions and the dielectric constants in the protein and in the water were set to 1 and 80, respectively. The ionic strength was set to 0.1 M. The ratio between the longest dimension of the rectangular finite-difference grid and that of the solute was set to 4.0. The linear PB equation was solved using a maximum of 1,000 iterations.

The entropy from the vibrational degrees of freedom was calculated by normal mode analysis (NMA) using the Amber *mmpbsa_py_nabnmode* program. To this aim, 200 configurations were selected; each configuration was energy minimized with a Generalized-Born solvent model (nmode_igb = 1) using a maximum of 50,000 steps and a target root-mean-square (rms) gradient of 10^{-4} kcal mol^{-1} Å^{-1}.

From the binding total binding free energies for for wild type and mutant HIV-1 PR excluding the entropic contributions, $\Delta\tilde{G}_{\text{WT}}$ and $\Delta\tilde{G}_{\text{mut}}$, respectively, the mutation-induced shift in binding free energy also denoted as relative binding free energy $\Delta\Delta G_{\text{bind}} = \Delta\tilde{G}_{\text{mut}} - \Delta\tilde{G}_{\text{WT}}$ was calculated. The entropic contributions were excluded as a previous study [56] indicates that the entropic contribution difference nearly cancels out when the protein-protein binding of single residue mutant is compared, and these findings were supported by our own results for the entropy. From the relative binding free energies, the

corresponding change in association constants, r, was evaluated. The change in binding constants was defined as the ratio

$$r \equiv K_a'/K_a \tag{8}$$

where Ka or $K_a^{'}$ denote the value of the association constant for the HIV-1 PR mutant or wild type, respectively. The change in binding constants was computed from

$$r = \exp(-\Delta\Delta G_{\text{bind}}/k_B T) \tag{9}$$

where k_B is the Boltzmann constant and T is the absolute temperature. On the other hand, Eqs. 8 and 9 were also used to convert experimental binding constants into corresponding relative binding free energies. For the change in binding constants from the simulations, not a single number but a range was given. The range was obtained by replacing $\Delta\Delta G_{\text{bind}}$ by $\Delta\Delta G_{\text{bind}} \pm \text{se}(\Delta\Delta G_{\text{bind}})$, where $\text{se}(\Delta\Delta G_{\text{bind}})$ denotes the standard error of the relative binding free energy. The same scheme was used to determine the range of r in our previous study [48].

The standard errors of the mean for the individual components to the binding free energy were computed by dividing the respective standard deviations by the square root of the number of configurations considered. The standard error of the absolute and the relative binding free energies were evaluated from error propagation.

In order to understand the inhibitor-residue interaction in more detail, the interaction energy was further decomposed into the contributions from each residue of the protease by using the theory of free energy decomposition [57].

Results and discussions

In order to understand the mechanisms underlying the binding of amprenavir to the wild-type protease and its variants, an energetic analysis using the MM-PBSA method was conducted. Molecular configurations obtained from MD simulations of the complexes in explicit water were used for the calculation of binding free energies. The production simulations of 20 ns carried out for these systems were stable on the basis of the total and potential energies of these systems (data not shown) and the root mean square deviation (RMSD) from the X-ray structures.

Structural stability

The RMS deviations for the back bone atoms from the corresponding X-ray crystal structure in the simulations with four different protonation states of the Asp25 dyad are shown in Fig. 4. The average root mean squared deviations for the backbone atoms from the corresponding X-ray crystal structure in the simulations with the four different protonation states of Asp25/Asp25′ are given in Table 1. The table shows that the RMSDs of the unprotonated systems are larger than that of the mono25, mono25′ and dipro systems while a similar dynamical behavior is observed for mono25, mono25′ and dipro (see Fig. 4). Their average RMSD values are 1.16, 1.17 and 1.17 Å for wild type mono25, mono25′ and dipro, respectively, with a deviation of lower than 0.17 Å from the mean. In contrast, the wild type unprotonated system exhibits an average RMSD value of 1.42 Å with a deviation of 0.15 Å from the mean. Similar results were obtained for the HIV-1 PR-BEA369 complex [14].

Although it may seem that the red curve is still evolving, however, considering the fluctuations the red curve actually shows no significant drift of the RMSD after 10 ns, so it does seem to have reached a plateau. There is roughly a 1 Å RMSD already present in the initial steps of the MD.The initial configuration corresponding to t = 0 in

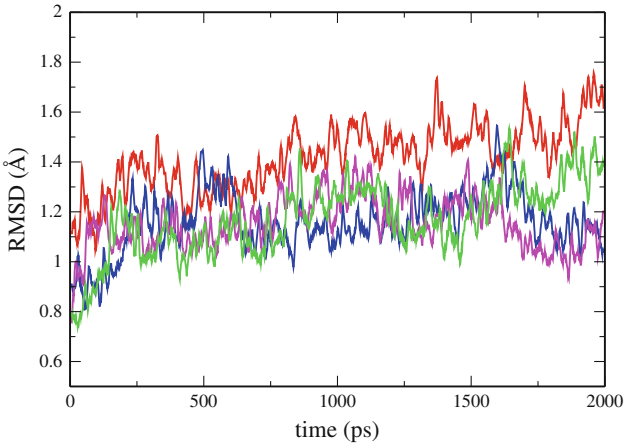

Fig. 4 Time evolution of root-mean-square deviations (RMSD) of backbone atoms relative to their initial configurations for wild type PR-inhibitor complexes with different protonation states for the Asp25 dyad. *Red* unpro (both Asp25 and Asp25′ deprotonated); *Blue* Mono25 (Asp25 protonated); *Magenta* Mono25′ (Asp25′ is protonated); *Green* dipro (protonated at both Asp25 and Asp25′)

Table 1 Average RMSD during the 20 ns production simulations of the protease–inhibitor complexes of fourdifferent protonation states. Standard errors of the mean are provided in parentheses

Variant	Unpro (Å)	Mono25 (Å)	Mono25′ (Å)	Dipro (Å)
WT	1.42 (0.15)	1.16 (0.14)	1.17 (0.12)	1.17 (0.16)
V32I	1.33 (0.14)	1.12 (0.15)	1.05 (0.13)	1.02 (0.12)
I50V	1.44 (0.18)	1.12 (0.12)	1.16 (0.13)	1.08 (0.15)
I54M	1.07 (0.12)	0.99 (0.12)	0.95 (0.11)	0.95 (0.11)
I54V	1.44 (0.17)	1.05 (0.14)	1.08 (0.12)	0.99 (0.12)
I84V	1.75 (0.23)	1.05 (0.11)	1.08 (0.16)	1.04 (0.13)
L90M	1.45 (0.18)	1.22 (0.16)	1.27 (0.18)	1.01 (0.12)

Table 2 Binding free energy of the protease–inhibitor complexes of four different protonation states

Variant	unpro	mono25	mono25′	dipro	Exp[a]
WT	−0.7 (0.5)	−15.3 (0.5)	−15.1 (0.5)	−19.0 (0.5)	−13.4 to −13.5
V32I	0.6 (0.6)	−13.9 (0.7)	−13.5 (0.7)	−18.2 (0.5)	−12.0 to −12.2
I50V	−4.4 (0.7)	−12.8 (0.6)	−12.6 (0.6)	−15.1 (0.6)	−11.4 to −11.6
I54M	−0.1 (0.6)	−14.2 (0.5)	−13.7 (0.5)	−17.6 (0.5)	−12.7 to −12.9
I54V	−1.3 (0.6)	−14.6 (0.7)	−14.6 (0.6)	−17.8 (0.6)	−12.8 to −13.0
I84V	1.7 (0.7)	−13.7 (0.6)	−14.0 (0.7)	−17.0 (0.6)	−12.3 to −12.6
L90M	−1.1 (0.5)	−15.4 (0.5)	−15.1 (0.5)	−18.2 (0.5)	−13.4 to −13.5

Values are given in kcal/mol. Standard errors of the mean are provided in parentheses

[a] Obtained from Ref. [11]

Fig. 4 is obtained after previous numerical steps including energy minimization and 1 ns MD simulation. So it is understandable that the "t = 0" configuration differs from experimental one. That the RMSD does not increase much more during the rest of the trajectory indicates that the RMSD is equilibrated at an early stage, as desirable.

Ranking of binding affinities for different protonation states and mutations

The binding free energies for the different HIV-1 PR variant/APV complexes in different protonation states are shown in Table 2.

Overall, the dipro systems show the highest and the unpro systems the lowest affinities. Table 2 compares the absolute binding free energies from our calculations with the experimental values. It is found that the dipro, the mono25, and the mono25′ systems show the same ranking as the experimental values whereas the unpro system shows a different ranking.

Binding mechanism depends on protonation state

The individual components of the binding free energy for the mono25, mono25′ and dipro systems are summarized in Table S2, Table 5 and Table S3. These tables show that the binding is favored by van der Waals and electrostatic interactions. The non-polar solvation free energy, which corresponds to the burial of SASA upon binding, also slightly favors the complex formation. However, the polar component of the solvation free energy and the entropy disfavor the complex formations. These findings agree with MM-PBSA studies for other protein-ligand complexes [48]. The individual components of the binding free energy are influenced by the protonation states of Asp25/Asp25′. As can be seen from Table 5, Table S2 and Table S3, the protonation state of Asp25/Asp25′ affects only slightly the van der Waals term but strongly the electrostatic and the polar solvation terms, as might be expected.

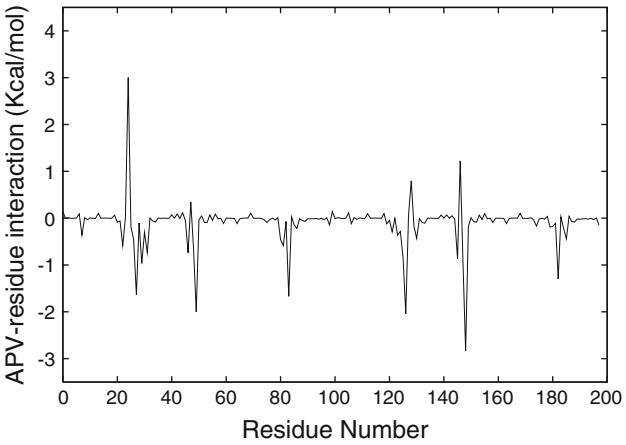

Fig. 5 Decomposition of ΔG on a per-residue basis for the wild type protein-inhibitor (APV) complex. The Asp25 dyad is in mono25′. Residues 1–99 and 100–198 correspond to residues 1–99 and 1′–99′, respectively

In order to gain insight into the effect of the protonation of Asp25/Asp25′ on the binding at the atomic level, the binding free energies were decomposed into contributions from each PR residue. The inhibitor-residue interaction spectrums of the four different protonation states systems are shown in Fig. 5 and Fig. S1. It is evident from the figures that the protonation state has a distinct influence on the protease-inhibitor interactions, i.e., the contributions from individual residues to the binding free energy. In all four states of protonation, significant contributions to the binding free energy come from residues Ala28/Ala28′, Asp25/Asp25′, Asp30/Asp30′, Ile47/Ile47′, Ile50/Ile50′ and Ile84/Ile84′.

Experimental protonation state from pK_a calculations

The effect of the protonation state on the binding affinity and the binding mechanism described above highlights the need to determine the experimentally relevant protonation state. Often it is assumed that the protonation state yielding

the highest affinity is the correct one [14]. However, there is no physical reason to assume this. Instead, the protonation state depends on the pH of the solution and the pK_a of the protonable sites. In order to pinpoint the likely protonation state at the experimental pH we calculated pKa values for the Asp dyad. With the growth of the number of experimentally determined pK_a values, it has become possible to develop very simple structure-based empirical methods to calculate pK_a shifts. One of such methods, PROPKA [58, 59] utilizes a simple model parameterized to estimate shifts in pK_a values due to hydrogen bonding, desolvation, and charge–charge interactions, based on a large training set of known pK_as [58]. Empirical methods, such as PROPKA, offer an attractive alternative to PB- or MD-based approaches because of the computational efficiency. A recent benchmark study [60] noted PROPKA as more accurate than PB-based methods, such as MCCE, MEAD, and UHBD. PROPKA predicts pK_a values with an overall root mean square deviation of 0.79 pH units based on calculations for five proteins, 'OMTTKY3', bovine pancreatic trypsin inhibitor, hen egg white lysozyme, RNase A, and RNase H. However, continuous constant PH MD (CPHMD) [61] simulation method is more accurate but more expensive than PROPKA. Current limitations noted by the developers include the assumption that intraligand interactions are included in the pK_a model value, while both pK_a shifts due to interligand interactions and the effects of side chain motion as well as other conformations are not considered. Recently, Lee and Crippen [62] have surveyed the sources of experimental pK_a values and then focussed on current methods for predicting them. They have discussed the statistical validity, and predictive power of methods as well as their accuracy. PROPKA determines the pK_a of an ionizable group through the application of an environmental perturbation, ΔpK_a, to the unperturbed pK_a value of the group, pK_{Model}

$$pK_a = pK_{Model} + \Delta pK_a \tag{10}$$

where pK_{Model} is the corresponding pK_a for an individual amino acid in water as inferred from experiments, and the shift ΔpK_a is assessed computationally. For each ionizable group, ΔpK_a comprises five terms that describe global (GlobalDes) and local desolvation (LocalDes), hydrogen bonds with side-chain groups (SDC-HB), hydrogen bonds with the amide backbone (BKB-HB), and interactions with charged groups (ChgChg),

$$\Delta pK_a = \Delta pK_{GlobalDes} + \Delta pK_{LocalDes} + \Delta pK_{SDC-HB} + \Delta pK_{BKB-HB} + \Delta pK_{ChgChg}. \tag{11}$$

Table 3 shows the pK_a values for the Asp dyad as obtained from PROPKA. The predicted pK_a values are 2.07–2.33 for Asp25 and 8.25–8.43 for Asp25′. Hence, at pH 5.6, where the binding affinities and the structures of the PR–APV complexes were studied experimentally, Asp25 is most likely deprotonated and Asp25′ is protonated, corresponding to state mono25′.

Table 3 pKa values of Asp25/Asp25′ in presence of inhibitor obtained from PROPKA [58]

Variant	Asp25	Asp25′
WT	2.19	8.28
V32I	2.13	8.35
I50V	2.06	8.25
I54M	2.07	8.27
I54V	2.19	8.34
I84V	2.33	8.25
L90M	2.07	8.43

Although the active-site Asp residues are related by a structural symmetric dyad in the unbound form, the catalytic mechanism may proceed via asymmetric protonation states [63]. The catalytic mechanism of HIV-1 PR has been extensively investigated by several approaches [12].

The most widely accepted mechanism for aspartic protease has been described by Suguna et al. [64]. The proposed mechanism is based on the crystal structure of the Rhizopys chinensis aspartic protease complexed with a reduced peptide inhibitor. The pH-rate profile of this enzyme implies that only one of the two active site aspartic acids is unprotonated in the active pH range. In the proposed mechanism the Asp group that is closer to the nucleophilic water molecule was assigned the negative charge. The nucleophilic water molecule held between the catalytic aspartates, after its activation by the negative aspartate side chain, attacks the carbonyl group in the substrate scissile bond to generate an oxyanion tetrahedral intermediate. Protonation of the scissile amide N atom and rearrangement result in the breakdown of the tetrahedral intermediate to the hydrolysis products. This catalytic mechanism for aspartic proteases is schematically shown in Fig. 3 in Ref. [12]. Adachi et al. [63] have shown a schematic diagram of the energy profile for the catalysis by HIV-1 protease (see Fig. 5 in Ref. [57]).

Our pK_a calculations suggest that Asp25 is ionized and Asp25′ is protonated. On the other hand, it is often assumed that the protonation state with most negative binding free energy is correct which would suggest that the correct protonation state is the diprotonated state here (also Asp25 protonated). To resolve this apparent controversy, we give a formula for the binding free energy which considers both protonation states to explicitly show that the affinity is determined by the protonation state (and not vice versa as often implied). Assuming that PR both in the unbound state as well as bound to APV exists in an equilibrium between the dipro and mono25′ state as determined by the pH and

the pK_a values of Asp25′, it can easily be shown that the binding free energy may be expressed as

$$\Delta G_{\text{bind}} = -k_B T ln \frac{e^{-\Delta G_{\text{mono,PI}}/k_B T} + 1}{e^{-\Delta G_{\text{mono,P}}/k_B T} + 1} + \Delta G_{\text{di}} - G_{\text{I}} \quad (12)$$

with

$$\Delta G_{\text{mono},x} = G_{\text{mono},x} - G_{\text{di},x}, x = \text{P}, \text{PI}. \quad (13)$$

and

$$\Delta G_{\text{di}} = G_{\text{di,PI}} - G_{\text{di,P}}. \quad (14)$$

Here, $G_{\text{mono,P}}$, $G_{\text{di,P}}$, $G_{\text{mono,PI}}$, or $G_{\text{di,PI}}$ denote the free energy of the free PR in the monoprotonated or the diprotonated state, or the free energy of the PR–APV complex in the monoprotonated or the diprotonated state, respectively. For the experimentally relevant pH (5.6) and the computed pK_a value of Asp25 ($\sim$2), Eq. 12 reduces to Eq. 14 with $G_{\text{PI}} = G_{\text{mono, PI}}$ and $G_{\text{P}} = G_{\text{mono, P}}$, showing that ΔG_{bind} should be computed using the monoprotonated state. Here we emphasize that whereas ΔG_{bind} determines the affinity, the protonation state is determined by $\Delta G_{\text{mono},x}$, the relation between the two being given by Eq. 12. This shows that inferring the protonation state (which is determined by $\Delta G_{\text{mono},x}$) from ΔG_{bind} is inappropriate.

Contribution of aspartic dyad to binding free energies

The catalytic aspartic dyad Asp25 /Asp25′ is expected to be crucial to the binding of inhibitor with the protease. Hence it is important to estimate the total contribution coming from the Asp25 dyad to the binding free energy. We found the total contribution from Asp25/Asp25′ to be attractive (−0.72 kcal/mol) for the dipro system but repulsive for the other systems, the repulsion being lowest for mono25′ (2.73 kcal/mol), intermediate for mono25 (3.65 kcal/mol), and highest for unpro (13.88 kcal/mol).

The individual contributions from the two Asp residues to the binding free energy are given in the following. For the dipro system, both Asp25 and Asp25′ contributed favorably and the contribution from Asp25 (−0.50 kcal/mol) was twice that of Asp25′ (−0.22 kcal/mol). For mono25′, both Asp25 and Asp25′ were repulsive, Asp25 being more repulsive (2.59 kcal/mol) than Asp25′ (0.14 kcal/mol). For the mono25 system, Asp25 yielded a favorable contribution of −0.25 kcal/mol which, however, was not sufficient to counteract the repulsion of 3.90 kcal/mol by Asp25′.

It is interesting to note that while the pK_a calculations suggest mono25′ as experimentally relevant protonation state, the aspartic dyad yields a repulsive contribution to the binding free energy in this state. This may be counterintuitive; however, as the overall binding free energy is found to be negative, the repulsive effect of the dyad is obviously overcompensated by attractive components from other residues.

Flexibility of individual residues for experimental protonation state

As our PROPKA calculations suggest that only Asp25′ is protonated for the wild-type as well as mutant variants of the protein-inhibitor complex, only results for the mono25′ system will be discussed in the following. The results for the other protonation states are described in the SI.

A measure for the flexibility of the individual residues are the corresponding B-factors. The B-factor (B) of a residue depends on the fluctuations of the corresponding atomic positions from their mean position, according to

$$B = \frac{8}{3N}\pi^2 \sum_i^N \langle |R_i - < R_i > |^2 \rangle. \quad (15)$$

here, N is the number of atoms, R_i is the position of the i-th atom, and $\langle R_i \rangle$ is the ensemble average of R_i.

The B-factors of the individual residues for WT and mutant APV/PR complexes for the mono25′ systems are shown in Fig. 6. Particularly small B-factors are observed for the catalytic dyad (4.1 Å^2 for Asp25 and 8.1 Å^2 for Asp25′). This is expected, as the catalytic function of these residues presumably requires a well-defined stable three-dimensional structure.

Figure S2 compares B-factors from our simulations with the experimental values. It appears that the mutations have a quite strong effect on the overall profile of the B-factors, both in the simulated and the experimental profiles. It is apparent that the experimental and simulated profiles differ. We have obtained somewhat higher B-factors

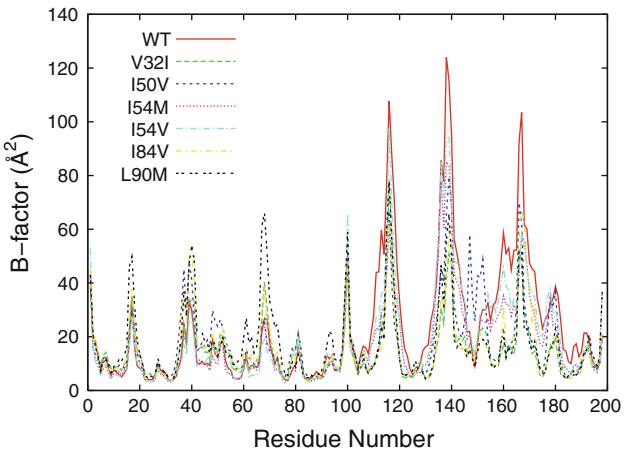

Fig. 6 B-factors for WT and mutant APV/PR complexes with Asp25 ionized and Asp25′ protonated. Residues 1–99 and 100–198 correspond to residues 1–99 and 1′−99′, respectively

compared to experiment for all the complexes. This difference could arise from crystallization effects in the experiments which would reduce the B-factors compared to solution; facing the strong effect of single site mutations on the B-factor profiles renders it possible that crystal contacts could be the origin of the deviation of the simulated from the experimental B-factors. However, overall a similar trend was observed in both simulations and experiments. Figures 6 and S2 show that flexible regions in the PR–APV complexes are the regions around residues 17, 40, 55, 68, 80, and 99 in chain A and the corresponding residues in chain B. This result is in accord with previous studies on the flexibility of PR [35].

Naively, an increase/decrease in the B-factor of a given residue is expected to correlate with a loss/gain of interactions of this residue with other residues. Following this idea, we shall relate mutation-induced changes in B-factors seen in our work to the discussions of structural changes by Shen et al. [11]. The B-factors referred to in the following discussion are given in Table 4.

V32I mutant

The V32I mutation adds one methyl group forming new van der Waals contacts with other hydrophobic side chains. Ile32 forms new hydrophobic contacts, not present for PR_{WT}, with the side chains of Val56, Leu76, and the main chain atoms of residues 77 – 78, while Ile32′ shows new interactions with the side chains of Ile47′, Ile50, and Val56′ in the flaps [11]. As expected from the new contacts formed by the mutated residues, the B-factor of these residues decreases (from 3.69 Å^2 for PR_{WT} to 3.65 Å^2 in the mutant case for residue 32 and, drastically, from 16.95 Å^2 for PR_{WT} to 4.56 Å^2 for the mutant complex). Two residues to which these new contacts are formed show a strong decrease in B-factors (21.86 Å^2 in the WT to 14.15 Å^2 in the mutant case for Ile47′ and 25.92 Å^2 in the WT to 10.72 Å^2 in the mutant complex). The other residues (Ile50, Val56, and residues 76–78) show a moderate increase in B-factors. This may indicate a weakening of some interactions due to a perturbation of the packing due to the newly introduced methyl group.

I50V mutant

Ile50 is located at the tip of the flap on each PR monomer. In PR_{WT}, Ile50/Ile50′ interacts with Pro81′/Pro81 and Thr80′/Thr80, as well as Ile47′/Ile47 and Ile54′/Ile54 in the flaps. The I50V mutation shortens the side chain by a methyl group, thereby removing the C–H···O interaction with the hydroxyl oxygen of Thr80′ and a van der Waals contact with Ile54′. In the other subunit, the mutation to Val50′ eliminates the C–H···O interaction with the hydroxyl of Thr80 and a hydrophobic contact with Pro81 [11]. As expected, the loss in contacts correlates with an increase in the B-factors of most of the residues involved (Ile/Val50, Ile/Val50′, Thr80, Pro81, and Ile54′). Only the B-factor of Thr80′ is reduced in the mutant complex.

Table 4 B-factors of selected residues for the WT and mutant APV-PR complexes in Å^2. The rightmost column indicates if the B-factor for the mutant cases is increased ("+") or reduced ("−") compared to the WT case

Residue	WT	V32I	
V32	3.70	3.65	−
I50	12.22	14.24	+
V56	4.96	8.03	+
L76	3.95	4.74	+
V77	3.76	5.62	+
G78	5.90	9.67	+
V32′	16.95	4.56	−
M47′	21.86	14.15	−
L56′	25.91	10.72	−
Residue	**WT**	**I50V**	
I50	12.22	23.80	+
T80	9.74	15.84	+
P81	15.79	20.91	+
I50′	9.17	25.84	+
I54′	29.98	33.89	+
T80′	33.97	30.78	−
Residue	**WT**	**I54M**	
I54	8.39	9.73	+
P79	8.30	8.35	+
T80	9.74	7.28	−
I54′	29.98	25.46	−
P79′	31.83	34.34	+
T80′	33.97	24.36	−
Residue	**WT**	**L90M**	
25	4.08	5.09	+
26	6.01	6.44	+
90	5.08	7.46	+
25′	8.12	7.18	−
90′	12.60	6.63	−

I54M mutant

The I54M mutation introduces a longer side chain. The Met54/54′ side chains form more hydrophobic contacts with Pro79/Pro79′ and Thr80/80′ in PR_{I54M} relative to PR_{WT}. According to Shen et al., the Ile54 to Met mutation "improves the contacts with the hydrophobic cluster,

Table 5 Free energy terms (kcal/mol) of binding of amprenavir to the wild-type and mutant variants of HIV-1 PR

Mutant	$\langle \Delta E_{vdW} \rangle$	$\langle \Delta E_{elec} \rangle$	$\langle \Delta G_{np} \rangle$	$\langle \Delta G_{pol} \rangle$	ΔG_{solv}[a]	$\Delta G_{pol,elec}$[b]	$\langle -T\Delta S_{tot} \rangle$	ΔG_{bind}
WT	−63.0 (0.1)	−61.6 (0.2)	−5.1 (0.01)	81.8 (0.2)	76.7 (0.2)	20.2 (0.3)	32.8 (0.3)	−15.1 (0.5)
V32I	−62.2 (0.1)	−64.2 (0.3)	−5.2 (0.01)	85.3 (0.2)	80.1 (0.2)	21.1 (0.4)	32.8 (0.3)	−13.5 (0.7)
I50V	−59.3 (0.1)	−63.4 (0.2)	−5.2 (0.01)	82.8 (0.2)	77.6 (0.2)	19.4 (0.3)	32.5 (0.3)	−12.6 (0.6)
I54M	−62.7 (0.2)	−60.2 (0.3)	−5.1 (0.01)	81.6 (0.2)	76.5 (0.2)	18.0 (0.4)	32.7 (0.3)	−13.7 (0.5)
I54V	−63.4 (0.2)	−59.0 (0.3)	−5.1 (0.01)	80.1 (0.2)	75.0 (0.2)	21.1 (0.4)	32.8 (0.3)	−14.6 (0.6)
I84V	−60.3 (0.2)	−63.1 (0.4)	−5.2 (0.01)	81.8 (0.3)	76.6 (0.3)	18.7 (0.5)	32.8 (0.4)	−14.0 (0.7)
L90M	−61.7 (0.2)	−60.0 (0.3)	−5.1 (0.01)	79.1 (0.2)	74.0 (0.3)	19.1 (0.4)	32.6 (0.5)	−15.1 (0.5)

Standard errors of the mean are given in parenthesis. Asp25′ is in mono-protonated state. Six water molecules closest to the ligand were considered in this calculation

[a] $\Delta G_{solv} = \Delta G_{np} + \Delta G_{pol}$, [b] $\Delta G_{pol,elec} = \Delta G_{pol} + \Delta E_{elec}$

although interatomic distance to residues 79–80/79′−80′ (are) increased“ [11]. The B-factors of the residues involved show a mixed behavior, being increased for half of the residues (residues 54, 79, and 79′) and decreased for the others (residues 80, 54′, and 79′).

L90M mutant

The mutation of Leu90 to Met means to substitute a longer side chain and introduces new van der Waals contacts with with residues Asp25-Thr26. The Met90/Met90′ side chains form close C–H/···O interactions with the carbonyl oxygen of the catalytic Asp25 and Asp25′ [11]. The new contact of residue 90′ strongly reduces the B-factor of this residue, while the other residues involved either only show a moderate decrease (residue Asp25′) or even an increase in the B-factor (residues 25, 26, and 90), the latter possibly indicating a perturbation of the packing due to the substitution of the longer side chain.

Shen et al. did not discuss specific changes in intramolecular interactions within PR for the I54V and the I84V mutant, so we have skipped these mutants in our discussion of B-factors.

Binding mechanism for experimental protonation state

In our current study, we are interested to evaluate the relative potency of APV against the wild-type and the mutant H IV-1 proteases and the molecular basis of drug resistance. In order to elucidate the binding mechanisms for the experimental protonation state (mono25′), we also provide the individual contributions to the binding free energies. Here, the contribution from the van der Waals or electrostatic interactions between the protease and the inhibitor, ΔE_{elec} or ΔE_{vdW}, respectively, the polar or nonpolar solvation free energy, ΔG_{pol} or G_{np}, respectively, the sum of ΔE_{elec} and ΔG_{pol} denoted as $\Delta G_{pol,elec}$, and the contribution from the configurational entropy of the binding partners, denoted as $-T\Delta S_{MM}$, were considered. The entropic contributions from the vibrational degrees of freedom were calculated using normal mode analysis.

Energetic components

The energetics of binding APV to the wild-type PR and its single mutant variants obtained from MM-PBSA calculations are shown in Table 5. The total binding free energies are found to range between −12.6 kcal/mol and −15.1 kcal/mol. The contributions favoring binding are the van der Waals interaction between the binding partners, being in the range −59.3 to −63.4 kcal/mol, and the intermolecular electrostatic energy in the range −59.0 to −64.2 kcal/mol for all protease-inhibitor complexes. The nonpolar interactions with the solvent including the contribution from the hydrophobic effect yield contributions in the range −5.0 kcal/mol for APV complexed with the wild type and the mutant variants of the protease. Association is opposed by an unfavorable desolvation of polar groups, yielding a contribution of 74.0 to 80.1 kcal/mol for APV complexed with wild type and mutant PR. As found for other systems [20, 30, 65], the unfavorable desolvation of polar groups is only partially compensated by favorable intermolecular electrostatic interactions. The sum of the contribution from the desolvation of polar groups and the intermolecular electrostatic interactions varies from 18.0 to 21.1 kcal/mol for the protease-inhibitor complexes.

Configurational entropy

Formation of macromolecular complexes is in general opposed by a loss in configurational entropy of the binding partners [48, 65, 66]. The corresponding contributions from the loss in entropy due to the translational, rotational, and vibrational degrees of freedom to the binding of free energy of the protease-inhibitor complexes were about 32.5 kcal/mol. This entropic component is often not

considered in MM/PBSA calculations, partly because, as observed here, it may nearly cancel out in computation-induced shifts in binding free energies which are often the main interest of such kind of studies [56]. Hence we did not include the entropic contribution in the calculation of relative binding free energies.

Mutation induced shifts in affinity

The mechanism underlying the mutation-induced changes in affinity may be elucidated from the variation of different components of the binding free energy upon mutations that can be deduced from Table 5. From the table, the predicted total binding free energies of the WT, PR_{V32I}, PR_{I50V}, PR_{I54M}, PR_{I54V}, PR_{I84V} and PR_{L90M}/APV complexes using single trajectory scheme are −15.1, −13.5, −12.6, −13.7, −14.6, −14.0 and −15.1 kcal/mol, respectively.

Relative binding free energies

The shifts in binding free energies due to mutations from our calculations as well as from experiment are given in Table 6. Compared to the PR_{WT}–APV complex, the mutants PR_{V32I}, PR_{I50V}, PR_{I54M}, PR_{I54V} and PR_{I84V} caused shifts in ΔG of 1.6, 2.5, 1.4, 0.5 and 1.1 kcal/mol in the binding free energy, respectively, which suggests that all these mutants bind less strongly to APV. This also explains why V32I, I50V, I54M, I54V, and I84V may cause drug resistance against APV. However, L90M does not lead to drug resistance against the inhibitor APV. V32I and I50V cause higher drug resistance compared to the other mutants. It has been shown experimentally that V32I causes a 10-fold and I50V a 30-fold reduction in affinity compared to the wild type PR [11].

Table 6 Relative binding free energy of the protease–inhibitor complexes for mono25′ system

Variant	$\Delta\Delta G_{sim}$ [a,b]	$\Delta\Delta G_{exp}$ [b,c]	r^{sim}	r^{exp}
V32I	1.6 (0.3)	1.4	9–24	10
I50V	2.3 (0.2)	2.1	33–67	30
I54M	1.4 (0.2)	0.7	7–15	3
I54V	0.5 (0.3)	0.7	1–4	3
I84V	1.1 (0.3)	1.1	4–9	6
L90M	0.0 (0.3)	0.0	0.6–2	1

Entropic contributions to the binding free energy were not included

[a] $\Delta\Delta G_{sim} = \Delta G_{WT} - \Delta G_{MUT}$

[b] Unit is in kcal/mol

[c] $\Delta\Delta G_{exp} = -K_b T \ln(r^{exp})$

Mutation-induced changes in binding constants and comparison to experiment

The mutation-induced shifts in binding constants (relative binding constants) are shown in Table 6. Compared to the PR_{WT}–APV complex, the association constant is decreased 9 to 24-fold for PR_{V32I}–APV, 33 to 67-fold for PR_{I50V}–APV, 7 to 45-fold for PR_{I54M}–APV, 1 to 4-fold for PR_{I54V}–APV and 4 to 9-fold for the PR_{I84V}–APV complex. No change in relative binding constant is observed for the L90M mutation. The ranking of the affinities found here corresponds to the experimental observations shown in the same table. Also, as in experiment, the key mutations are found to be V32I and I50V. Most of the relative binding constants and relative affinities for the association of HIV-1 PR variants with APV according to Eqs. 8 and 9 show even quantitative agreement with the experimental values if the statistical errors are considered. An exception is the relative binding constant for PR_{I54M} which is overestimated by a factor of two to five.

The mechanisms underlying drug resistance may be deduced from a decomposition of the binding free energy given in Table 5.

V32I mutant

Val32 belongs to the S2 pocket in the active site cavity and forms van der Waals interactions with APV. Its mutation to Ile adds one methyl group which may reduce the volume of the active site cavity. A 10-fold decrease in binding affinity for APV-PR_{V32I} was detected experimentally. However, no significant alterations in the interactions with APV where detected from structural inspection [11]. A shift in binding free energy of 1.4 kcal/mol and a 15-fold decrease in affinity compared to the WT, in agreement with the experimental data considering the standard error, is detected from our calculations. Table 5 shows that this mutant exhibits a shift in the van der Waals energy by 0.8 kcal/mol relative to the wild type, and a shift in the electrostatic energy by −2.6 kcal/mol. The nonpolar component of the solvation free energy is barely affected by the mutation. However, V32I causes an increase in the polar solvation energy which opposes binding by +3.5 kcal/mol and, thus, yields the largest contribution supporting drug resistance.

I50V mutant

Ile50 and Ile50′ reside at the tip of the flap of the corresponding PR monomer where their side chains form hydrophobic contacts with APV [11]. The mutation of Ile50 to Val50 shortens the side chain by a methyl group. In the crystal structure of APV bound to PR_{WT} as well as

the I50V mutant, APV shows two alternative conformations with relative occupancies of 0.7/0.3 for the WT and 0.6/0.4 for the mutant. In the mutant complex, a hydrogen bond between APV's aniline group in the major conformation of the inhibitor and the carbonyl oxygen of Asp30 is elongated compared to the WT complex. Shen et al. write that this elongated hydrogen bond contributes to decreased APV inhibition of PR-I50V without discussing other hydrogen bonds [11].

Closer inspection of their data, though, reveals that, inversely, some other hydrogen bonds are shortened or newly created in the mutant. A new hydrogen bond, not present in the WT PR suggested from a distance between the donor and acceptor above 3.5 Å, is formed between APV's aniline group in the minor conformation of the inhibitor and the carbonyl oxygen of Asp30. A shortening compared to WT PR is observed for the hydrogen bonds between APV/N1 in the major conformation of the inhibitor and a crystal water, between APV/O18 and Asp25/OD2 or APV/O18 and Asp25′/OD2 in the major or minor conformation of the inhibitor, respectively, between APV/O18 and Asp25/OD1 in the major conformation of the inhibitor, between a crystal water and APV/O10 in the minor conformation of the inhibitor, as well as between APV/O26 and Asp30/′OD1 or APV/O26 and Asp30/OD1 in the major and minor conformation of the inhibitor, respectively [11].

In MM/PBSA calculations, the energetic contribution of hydrogen bonds between the solutes or between the solutes and crystal waters are included in the electrostatic energy, E_{elec}. Indeed, the shortening of several hydrogen bonds in the structure correlates with a shift of −1.8 kcal/mol in E_{elec} compared to PR_{WT}. This change is only partially compensated by a shift of 1.0 kcal/mol for the polar solvation free energy compared to the WT complex, leading to $\Delta G_{pol,elec} = -0.8$ kcal/mol.

An increase in the interatomic distance of 3.4–3.5 Å suggests that hydrophobic interactions between the tetrahydrafuran (THF) group of APV and Ile50′ are lost in the mutant case. As shown in Table 7, this is reflected in a change in ΔE_{vdw} for residue 50′ from −2.56 kcal/mol for the WT complex to −1.98 kcal/mol for the mutant complex, mainly arising from the interactions of APV with the side chains of this residue (change from −1.84 kcal/mol for the WT to −1.29 kcal/mol for the mutant case). Also other residues loose van der Waals interactions with APV, as indicated from a total change in ΔE_{vdw} by 3.7 kcal/mol. Hence, the increase in ΔE_{vdw} overcompensates the decrease in $\Delta G_{pol,elec}$, as the origin of the drug resistance.

I54M and I54V mutants

The I54M mutation introduces a longer side chain such that nearby main chain atoms are shifted relative to their

Table 7 Decomposition of ΔG on a per-residue basis

Residue	S_{vdW}	B_{vdW}	T_{vdW}	S_{ele}	B_{ele}	T_{ele}	S_{PB}	B_{PB}	T_{PB}	T_{PBTOT}
WT/APV										
Ala28	−0.57	−1.20	−1.77	0.07	−0.12	−0.05	−0.08	0.27	0.19	−1.64
Ile50	−1.39	−0.47	−1.86	−0.87	0.29	−0.58	0.75	−0.32	0.43	−2.00
Ile84	−1.47	−0.14	−1.61	0.18	−0.31	−0.13	−0.29	0.36	0.07	−1.67
Ala28′	−0.71	−1.33	−2.04	0.04	−0.83	−0.79	−0.06	0.85	0.79	−2.04
Ile50′	−1.84	−0.72	−2.56	−0.81	−0.56	−1.37	0.73	0.36	1.09	−2.84
Ile84′	−1.17	−0.10	−1.27	0.01	0.08	0.09	−0.11	−0.02	−0.13	−1.30
V32I/APV										
Ala28	−0.55	−1.20	−1.75	0.06	−0.14	−0.08	−0.06	0.36	0.30	−1.53
Ile50	−1.37	−0.47	−1.84	−0.74	0.50	−0.24	0.68	−0.43	0.25	−1.82
Ile84	−1.42	−0.06	−1.48	0.21	−0.28	−0.07	−0.28	0.33	0.05	−1.58
Ala28′	−0.68	−1.20	−1.88	0.04	−0.36	−0.32	−0.07	0.71	0.64	−1.56
Ile50′	−1.88	−0.82	−1.70	−0.88	−0.48	−1.36	0.75	0.29	1.04	−3.04
Ile84′	−0.89	−0.08	−0.97	0.02	0.04	0.06	−0.15	0.01	−0.14	−1.06
I50V/APV										
Ala28	−0.65	−1.03	−1.68	0.04	0.09	0.13	−0.07	0.16	0.09	−1.47
Val50	−1.07	−0.50	−1.57	−0.85	0.73	−0.12	0.83	−0.62	0.21	−1.48
Ile84	−1.61	−0.08	−1.69	0.21	−0.30	−0.09	−0.28	0.39	0.11	−1.76
Ala28′	−0.71	−1.31	−2.02	0.03	−0.64	−0.61	−0.05	0.71	0.66	−1.97
Val50′	−1.29	−0.69	−1.98	−0.82	−0.50	−1.32	0.79	0.24	1.03	−2.28
Ile84′	−1.10	−0.05	−1.15	0.04	0.05	0.09	−0.15	0.02	−0.13	−1.24

Table 7 continued

Residue	S_{vdW}	B_{vdW}	T_{vdW}	S_{ele}	B_{ele}	T_{ele}	S_{PB}	B_{PB}	T_{PB}	T_{PBTOT}
I54M/APV										
Ala28	−0.61	−0.96	−1.57	0.05	0.07	0.12	−0.09	0.31	0.22	−1.23
Ile50	−1.33	−0.45	−1.78	−0.82	0.59	−0.23	0.69	−0.43	0.26	−1.74
Ile84	−1.79	−0.19	−1.98	0.24	−0.31	−0.07	−0.33	0.40	0.07	−1.99
Ala28′	−0.68	−1.30	−1.98	0.04	−0.59	−0.55	−0.06	0.74	0.68	−1.86
Ile50′	−1.82	−0.90	−2.72	−0.94	−0.47	−1.41	0.71	0.31	1.02	−3.10
Ile84′	−1.18	−0.10	−1.28	0.04	0.07	0.11	−0.11	−0.04	−0.15	−1.32
I54V/APV										
Ala28	−0.56	−1.15	−1.71	0.06	−0.17	−0.11	−0.06	0.36	0.30	−1.52
Ile50	−1.24	−0.52	−1.76	−0.83	0.58	−0.25	0.69	−0.45	0.24	−1.77
Ile84	−1.48	−0.14	−1.62	0.12	−0.29	−0.17	−0.21	0.35	0.14	−1.65
Ala28′	−0.75	−1.37	−2.12	0.06	−0.91	−0.85	−0.07	0.93	0.86	−2.11
Ile50′	−1.68	−0.76	−2.44	−0.90	−0.52	−1.42	0.75	0.29	1.04	−2.82
Ile84′	−1.03	−0.09	−1.12	0.03	0.09	0.12	−0.14	−0.01	−0.15	−1.15
I84V/APV										
Ala28	−0.59	−1.05	−1.64	0.06	−0.14	−0.08	−0.08	0.30	0.22	−1.50
Ile50	−1.32	−0.46	−1.78	−0.75	0.52	−0.23	0.69	−0.43	0.26	−1.74
Val84	−1.12	−0.16	−1.28	0.21	−0.34	−0.13	−0.29	0.43	0.14	−1.28
Ala28′	−0.74	−1.39	−2.13	0.07	−0.94	−0.87	−0.07	0.94	0.87	−2.13
Ile50′	−1.78	−0.76	−2.54	−0.82	−0.53	−1.35	0.75	0.32	1.07	−2.81
Val84′	−0.70	−0.11	−0.81	0.04	0.07	0.11	−0.11	0.07	−0.04	−0.72
L90M/APV										
Ala28	−0.60	−1.03	−1.63	0.05	0.03	0.08	−0.06	0.22	0.16	−1.40
Ile50	−1.31	−0.45	−1.76	−0.74	0.53	−0.21	0.68	−0.45	0.23	−1.75
Val84	−1.70	−0.19	−1.89	0.18	−0.32	−0.14	−0.22	0.41	0.19	−1.84
Ala28′	−0.74	−1.39	−2.13	0.07	−0.98	−0.91	−0.07	0.93	0.86	−2.18
Ile50′	−1.86	−0.83	−2.69	−0.81	−0.53	−1.34	0.73	0.30	1.03	−3.00
Ile84′	−1.02	−0.09	−1.11	0.03	0.07	0.10	−0.12	−0.04	−0.16	−1.17

Energies shown as contributions from the van der Waals (vdW), electrostatic (ele), and polar solvation energy (PB) of side-chain (S), backbone (B), as well as the sum of them (T) for PR-inhibitor complexes. All values are given in kcal/mol

positions in PR_{WT} [11]. Resistance of the PR_{I54M} is mainly caused by a change in ΔE_{el} by about 1.4 kcal/mol compared to the wild type. Minor shifts in ΔG_{vdW} (0.3 kcal/mol) and ΔG_{pol} (0.2 kcal/mol) also contribute to the drug resistance. Inversely, substituting Ile54 by valine means to introduce a shorter side chain. Similarly as for the I54M mutant, the main factor leading to resistance of PR_{I54V} against APV arises from a shift in ΔE_{el}. The shift in ΔE_{el} (2.6 kcal/mol) is larger than for PR_{I54M} but partially compensated by changes in ΔG_{pol} of −1.7 kcal/mol and in ΔE_{vdW} by −0.4 kcal/mol.

I84V mutant

The mutation of Ile84 to Val removes a methylene moiety, which can reduce interactions with APV. PR_{WT} shows van der Waals contacts between $C_{\delta 1}$ of Ile84 and the benzyl and aniline moieties of APV and from $C_{\delta 1}$ of Ile84' to the isopropyl group of APV. These interactions are lost in the PR_{I84V} mutant structure as the interatomic distances are increased to above 4.3 Å [11]. As shown in Table 7, this is reflected in a change of ΔE_{vdw} for residue 84 from −1.61 kcal/mol in the WT to −1.28 kcal/mol in the mutant case and for residue 84′ from −1.27 kcal/mol for the WT to −0.81 kcal/mol for the mutant complex. The change is due to the change in the interactions of the corresponding side chains with APV (shift of 0.35 kcal/mol for residue 84 and 1.1 kcal/mol for residue 84′) and only slightly compensated by opposing shifts in the interactions of the respective backbone atoms with APV (shift of −0.2 kcal/mol for residue 84 and −0.1 kcal/mol for residue 84′). Also other residues loose van der Waals interactions with APV, indicated by a total shift of 2.7 kcal/mol in ΔE_{vdW}. The shift in van der Waals energies, though, is partially

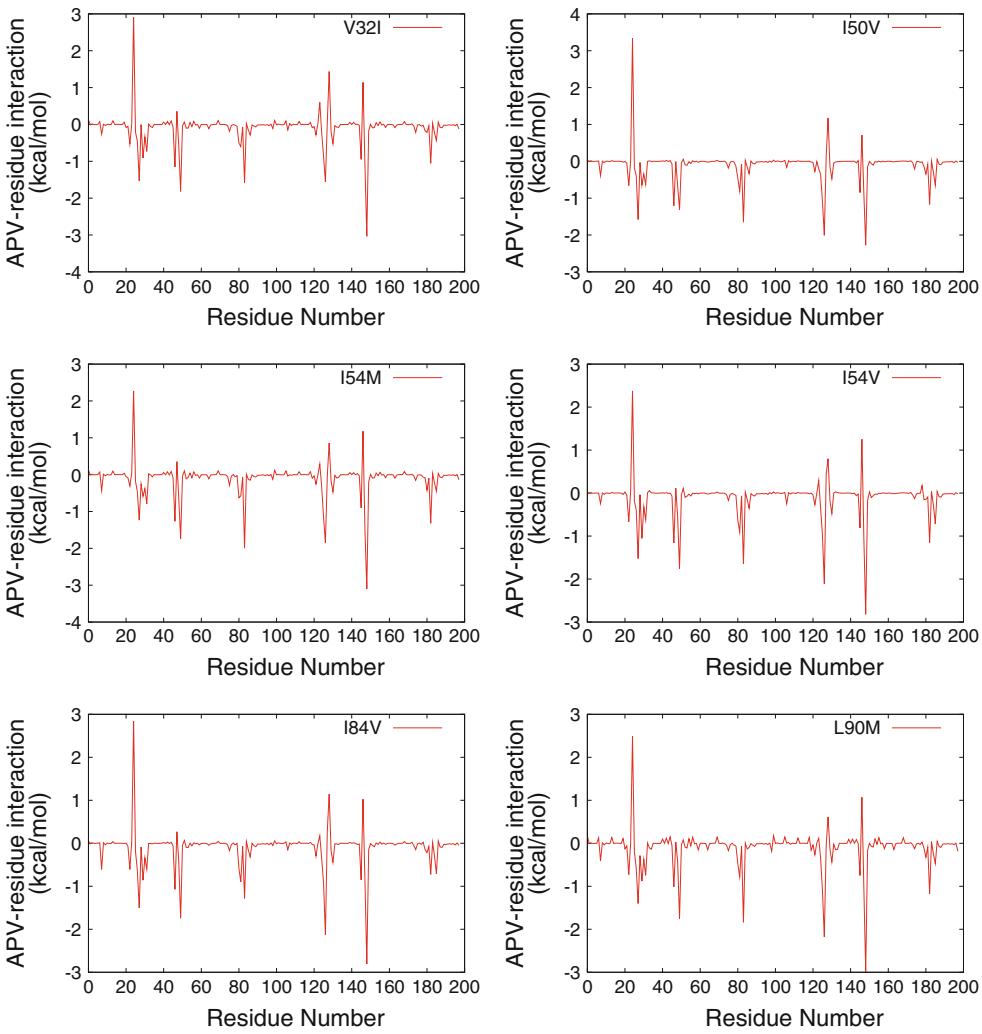

Fig. 7 Decomposition of ΔG on a per-residue basis for the mutant variant protease-inhibitor (APV) complex. Residues 1–99 and 100–198 correspond to residues 1–99 and 1′−99′, respectively

compensated by a change in the electrostatic PR–inhibitor interactions ΔE_{elec} of −1.5 kcal/mol compared to the wild-type, such that the total change in binding free energy is comparatively small (1.1 kcal/mol).

L90M mutant

Leu90 resides at the short α-helix outside of the active side cavity [11]. Its mutation to Met does not lead to any change in binding free energy compared to the wild-type. This is because the increase in van der Waals (1.3 kcal/mol) and gas phase electrostatic energies (1.6 kcal/mol) is counter balanced by an decreased polar component of the solvation energy (−2.7 kcal/mol).

Contributions from individual residues to the binding free energy

To acquire a more detailed insight into the basis of the resistance due to the single point mutations, the binding free energy was further decomposed into a per residue basis to generate an inhibitor-residue interaction spectra shown in Fig. 7. This is extremely useful to understand the drug resistant mechanism of V32I, I50V, I54V, I54M, I84V, and L90M to APV at the atomic level. From Fig. 7 it is clear that the overall interaction spectrums of all the complexes are quite similar. The attractive contributions mainly come from six groups around Ala28/Ala28′, Ile50/Ile50′, and Ile84/Ile84′. The repulsive contributions mainly come from Asp25, Asp30′ and Gly48′. From the analysis in Fig. 5, the residues contributing the most important favorable interactions may be inferred. The most important residues among these are listed in Table 7. Interestingly, this list includes residues 50 and 84 where two out of the five drug-resistant mutations considered in this paper occurred. The other residues in this list provide likely sites for future drug-resistant mutations. Interestingly, the mutations not only affect the mutated residue's contribution to the binding free energy but also contributions from other residues, indicating non-local effects of the

mutations. For example, the I50V mutation not only decrease the size of the contribution from residues 50 and 50′ but also the size of the contributions of residues Ala28, Ala28′, and Ile84′.

Dissection into backbone and side chain contributions for selected residues

A further dissection of contributions from individual residues into contributions from the backbone and the side chain, as well as corresponding van der Waals and electrostatic interactions and polar solvation free energies is given in Table 7. Six residues which contribute most favorably to the binding free energies are listed. For instance, the results show that for the I50 V mutant the decrease in the size of the contribution from residue 50 mainly arises from the decrease in the van der Waals interactions from the side chain of this residue.

Conclusion

In the present work, we have studied the binding of V32I, I50V, I54M, I54V, I84V, and I90M HIV-1 PR to amprenavir, using a combination of 20-ns MD simulations in explicit water and rescoring of the resulting configurations with an implicit solvent model. We have also investigated the effect of the protonation state of the aspartic dyad of HIV-1 PR on the structural stability and binding affinity of the PR–APV complex. Our results reveal that the protonation state of Asp25/Asp25′ strongly affects the dynamical behavior of the complex, the binding affinity and inhibitor-residue interactions. This highlights the importance of predicting the experimentally relevant protonation state. Calculations using PROPKA suggest the protonation to be mono25′. This protonation state was thus mainly considered in our study. Mutation induced changes in binding affinities are in agreement with the experimental findings. The decomposition of the binding free energy reveals the mechanisms underlying binding and drug resistance. Drug resistance arises from an increase in the energetic contribution from the van der Waals interactions between APV and PR (V32I, I50V, and I84V mutant) or a rise in the energetic contribution from the electrostatic interactions between the inhibitor and its target (I54M and I54V mutant). For the V32I mutant, also an increased free energy for the polar solvation contributes to the drug resistance. For the L90M mutant, a rise in the van der Waals energy for APV–PR interactions is compensated by a reduction in the polar solvation free energy such that the net binding affinity remains unchanged. Detailed understanding of the mechanisms underlying drug resistance might assist in the design of new inhibitors against HIV-1 PR variants that are resistant against current drugs.

Supporting information available

Free energy terms for the binding of amprenavir to the wild-type and mutant variants of HIV-1 PR for the mono25 and dipro systems, as well as a decomposition of the binding free energy for individual residues for the wild type protein-inhibitor (APV) complex for the mono25, dipro, and unpro systems.

Acknowledgements The work was supported by the Federal Ministry of Education and Research (BMBF), Germany. The authors thank Reinhard Lipowsky for support. P. K. is thankful to Dr. Siegfried Höfinger, University of Bologna, Italy for discussion.

References

1. Darke PL, Leu CT, Davis LJ, Heimbach JC, Diehl RE, Hill WS, Dixon RA, Sigal IS (1989) Human immunodeficiency virus protease. Bacterial expression and characterization of the purified aspartic protease. J Biol Chem 264:2307–2312
2. Seelmeir S, Schmidt H, Turk V, VonDer Helm K (1988) Human immunodeficiency virus has an aspartic-type protease that can be inhibited by pepstatin A. Proc Natl Acad Sci USA 85:6612–6616
3. Mous J, Heimer EP, Le Grice SJJ (1988) Processing protease and reverse transcriptase from human immunodeficiency virus type I polyprotein in Escherichia coli. J Virol 62:1433–1436
4. Hornak V, Okur A, Rizzo RC, Simmerling C (2006) HIV-1 protease flaps spontaneously open and reclose in molecular dynamics simulations. Proc Natl Acad Sci USA 103:915–920
5. Chang CA, Trylska J, Tozzini V, McCammon JA (2007) Binding pathways of ligands to HIV-1 protease: corase-grained and atomistic simulations. Chem Biol Drug Des 69:5–13
6. Wood E, Hogg RS, Yip B, Moore D, Harringan PR, Montaner JS (2007) Superior virological response to boosted protease inhibitor-based highly active antiretroviral therapy in an observational treatment programme. HIV Med 8:80–85
7. Walker BD, Burton DR (2008) Toward an AIDS vaccine. Science 320:760–764
8. Foulkes-Murzycki JE, Scott WR, Schiffer CA (2007) Hydrophobic sliding: a possible mechanism for drug resistance in human immunodeficiency virus type 1 protease. Structure 15:225–233
9. Shafer RW, Schapiro JM (2008) HIV-1 drug resistance mutations: an updated framework for the second decade of HAART. AIDS Rev 10:67–84
10. Vergne L, Peeters M, Mpoudi-Ngole E, Bourgeois A, Liegeois F, Toure-Kane C, Mboup S, Mulanga-Kabeya C, Saman E, Jourdan J, Reynes J, Delaporte E (2000) Genetic diversity of protease and reverse transcriptase sequences in non-subtype-B human immunodeficiency virus type 1 strains: evidence of many minor drug resistance mutations in treatment-naive patients. J Clin Microbiol 38:3919–3925
11. Shen C-H, Wang Y-F, Kovalevsky AY, Harrison RW, Weber IT (2010) Amprenavir complexes with HIV-1 protease and its drug-resistant mutants altering hydrophobic clusters. FEBS J 277:3699–3714

12. Brik A, Wong CH (2003) HIV-1 protease: mechanism and drug discovery. Org Biomol Chem 1:5–14
13. Smith R, Brereton IM, Chai RY, Kent SBH (1996) Ionization states of the catalytic residues in HIV-1 protease. Nat Struct Biol 3:946–950
14. Chen J, Yang M, Hu G, Shi S, Yi C, Zhang Q (2009) Insights into the functional role of protonation states in the HIV-1 protease-BEA369 complex: molecular dynamics simulations and free energy calculations. J Mol Model 15:1245–1252
15. Chen X, Tropsha A (1995) Relative binding free energies of peptide inhibitors of HIV-1 protease: the influence of the active site protonation state. J Med Chem 38:42–48
16. Wittayaranakul K, Aruksakunwong O, Saen-oon S, Chantratita W, Parasuk V, Sompornpisut P, Hannongbua S (2005) Insights into saquinavir resistance in the G48V HIV-1 protease: quantum calculations and molecular dynamic simulations. Biophys J 88:867–879
17. Wittayanarakul K, Hannongbua S, Feig M (2008) Accurate prediction of protonation state as a prerequisite for reliable MM-PB(GB)SA binding free energy calculations of HIV-1 protease inhibitors. J Comput Chem 29:673–685
18. Yamazaki T, Nicholson LK, Wingfield P, Stahl SJ, Kaufman JD, Eyermann CJ, Hodge CN, Lam PYS, Torchia DA (1994) NMR and X-ray evidence that the HIV protease catalytic aspartyl groups are protonated in the complex formed by the protease and a non-peptide cyclic urea-based inhibitor. J Am Chem Soc 116:10791–10792
19. Wang W, Kollman PA (2000) Free energy calculations on dimer stability of the HIV protease using molecular dynamics and a continuum solvent model. J Mol Biol 303:567–582
20. Chen J, Zhang S, Liu X, Zhang Q (2010) Insights into drug resistance of mutations D30N and I50V to HIV-1 protease inhibitor TMC-114: free energy calculation and molecular dynamic simulation. J Mol Model 16:459–468
21. Clavel F, Hance AJ (2004) HIV drug resistance. New Engl J Med 350:1023–1035
22. Wu TD, Schiffer CA, Gonzales MJ, Taylor J, Kantor R, Chou S, Israelski D, Zolopa AR, Fessel WJ, Shafer RW (2003) Mutation patterns and structural correlates in human immunodeficiency virus type 1 protease following different protease inhibitor treatments. J Virol 77:4836–4847
23. Johnson VA, Brun-Vezinet F, Clotet B, Gunthard HF, Kuritzkes DR, Pillay D, Schapiro JM, Richman DD (2008) Update of the drug resistance mutations in HIV-1. Top HIV Med 16:138–145
24. Wang W, Kollman PA (2001) Computational study of protein specificity: the molecular basis of HIV-1 protease drug resistance. Proc Natl Acad Sci USA 98:14937–14942
25. Kollman PA (1993) Free energy calculations: applications to chemical and biochemical phenomena. Chem Rev 93:2395–2417
26. Lybrand T, McCammon JA, Wipff G (1986) Theoretical calculation of relative binding affinity in host-guest systems. Proc Natl Acad Sci USA 83:833–835
27. Jayaram B, Sprous D, Young MA, Beveridge DL (1998) Free energy analysis of the conformational preferences of A and B forms of DNA in solution. J Am Chem Soc 120:10629–10633
28. Vorobjev YN, Almagro JC, Hermans J (1998) Discrimination between native and intentionally misfolded conformations of proteins: ES/IS, a new method for calculating conformational free energy that uses both dynamics simulations with an explicit solvent and an implicit solvent continuum model. Proteins 32:399–413
29. Kollman PA, Massova I, Reyes C, Kuhn B, Huo S, Chong L, Lee M, Lee T, Duan Y, Wang W, Donini O, Cieplak P, Srinivasan J, Case DA, Cheatham TE (2000) Calculating structures and free energies of complex molecules: combining molecular mechanics and continuum models. Acc Chem Res 33:889–897
30. Kuhn B, Kollman PA (2000) Binding of a diverse set of ligands to avidin and streptavidin: an accurate quantitative prediction of their relative affinities by a combination of molecular mechanics and continuum solvent models. J Med Chem 43:3786–3791
31. Rastelli G, Rio AD, Degliesposti G, Sgobba M (2010) Fast and accurate predictions of binding free energies using MM-PBSA and MM-GBSA. J. Comput. Chem. 31:797–810
32. Reyes CM, Kollman PA (2000) Investigating the binding specificity of U1A-RNA by computational mutagenesis. J Mol Biol 295:1–6
33. Reyes CM, Kollman PA (2000) Structure and thermodynamics of RNA-protein binding: using molecular dynamics and free energy analyses to calculate the free energies of binding and conformational change. J Mol Biol 297:1145–1158
34. Chen X, Weber IT, Harrison RW (2004) Molecular dynamics simulations of 14 HIV protease mutants in complexes with indinavir. J Mol Model 10:373–381
35. Hou T, McLaughlin WA, Wang W (2007) Evaluating the potency of HIV-1 protease drugs to combat resistance. Proteins 71:1163–1174
36. Stoica I, Sadiq SK, Coveney PV (2008) Rapid and accurate prediction of binding free energies for saquinavir-bound HIV-1 proteases. J Am Chem Soc 130:2639–2648
37. Hu GD, Zhu T, Zhang SL, Wang D, Zhang QG (2010) Some insights into mechanism for binding and drug resistance of wild type and I50V V82A and I84V mutations in HIV-1 protease with GRL-98065 inhibitor from molecular dynamic simulations. Eur J Med Chem 45:227–235
38. Cai Y, Schiffer CA (2010) Decomposing the energetic impact of drug resistant mutations in HIV-1 protease on binding DRV. J Chem Theory Comput 6:1358–1368
39. Hou T, Yu R (2007) Molecular dynamics and free energy studies on the wild-type and double mutant HIV-1 protease complexed with amprenavir and two amprenavir-related inhibitors: mechanism for binding and drug resistance. J Med Chem 50:1177–1188
40. Wang J, Morin P, Wang W, Kollman PA (2001) Use of MM-PBSA in reproducing the binding free energies to HIV-1 RT of TIBO derivatives and predicting the binding mode to HIV-1 RT of efavirenz by docking and MM-PBSA. J Am Chem Soc 123:5221–5230
41. Worch R, Bökel C, Höfinger S, Schwille P, Weidemann T (2010) Focus on composition and interaction potential of single-pass transmembrane domains. Proteomics 10:4196–4208
42. Kar P, Seel M, Weidemann T, Höfinger S (2009) Theoretical mimicry of biomembranes. FEBS Lett 583:1909–1915
43. Hornak V, Abel R, Okur A, Strockbine B, Roitberg A, Simmerling C (2006) Comparison of multiple amber force fields and development of improved protein backbone parameters. Proteins 65:712–725
44. Wang J, Wolf RM, Caldwell JW, Kollman PA, Case DA (2004) Development and testing of a general AMBER force field. J Comput Chem 25:1157–1174
45. Jakalian A, Jack DB, Bayly CI (2002) Fast, efficient generation of high-quality atomic charges. AM1-BCC model: II. Parameterization and validation. J Comput Chem 23:1623–1641
46. Wang J, Wang W, Kollman PA, Case DA (2006) Automatic atom type and bond type perception in molecular mechanical calculations. J Mol Gra Model 25:247–260
47. Case DA, Cheatham T, Darden T, Gohlke H, Luo R, Merz KM Jr, Onufriev A, Simmerling C, Wang B, Woods R (2005) The Amber biomolecular simulation programs. J Computat Chem 26:1668–1688
48. Kar P, Lipowsky R, Knecht V (2011) Importance of polar solvation for cross-reactivity of antibody and its variants with steroids. J Phys Chem B 115:7661–7669
49. Jorgensen WL, Chandrasekar J, Madura JD, Impey R, Klein K (1983) Comparison of simple potential functions for simulating liquid water. J Chem Phys 79:926–935

50. Ryckaert J-P, Ciccotti G, Berendsen HJC (1977) Numerical integration of the cartesian equations of motion of a system with constraints: molecular dynamics of n-alkanes. J Comput Phys 23:327–341
51. Darden T, York D, Pedersen L (1993) Particle mesh Ewald—an Nlog(N) method for Ewald sums in large systems. J Chem Phys 98:10089–10092
52. Sitkoff D, Sharp KA, Honig B (1994) Accurate calculation of hydration free energies using macroscopic solvent models. J Phys Chem 98:1978–1988
53. Weise J, Shenkin PS, Still WC (1999) Fast, approximate algorithm for detection of solvent-inaccessible atoms. J Comput Chem 20:217–230
54. Swanson JM, Henchman RH, McCammon JA (2004) Revisiting free energy calculations: a theoretical connection to MM/PBSA and direct calculation of the association free energy. Biophys J 86:67–74
55. Kongsted J, Ryde U (2009) An improved method to predict the entropy term with the MM/PBSA approach. J Comput Aided Mol Des 23:63–71
56. Massova I, Kollman PA (1999) Computational alanine scanning to probe protein-protein interactions: a novel approach to evaluate binding free energies. J Am Chem Soc 36:8133–8143
57. Gohlke H, Kiel C, Case DA (2003) Insights into protein-protein binding by free energy calculation and free energy decomposition for the Ras–Raf and Ras–RalGDS complexes. J Mol Biol 330:891–913
58. Li H, Robertson AD, Jensen JH (2005) Very fast empirical prediction and interpretation of protein pKa values. Proteins 61:704–721
59. Bas DC, Rogers DM, Jensen JH (2008) Very fast prediction and rationalization of pK_a values for protein–ligand complexes. Proteins 73:765–783
60. Davies MN, Toseland CP, Moss DS, Flower DR (2006) Benchmarking pK_a prediction. BMC Biochem 7:18
61. Khandogin J, Brooks CL III (2005) Constant pH molecular dynamics with proton tautomerism. Biophys J 89:141–157
62. Lee AC, Crippen GM (2009) Predicting pK_a J. Chem Inf Model 49:2013–2033
63. Adachi M, Ohhara T, Kurihara K, Tamada T, Honjo E, Okazaki N, Arai S, Shoyama Y, Kimura K, Maatsumura H, Sugiyama S, Adachi H, Takano K, Mori Y, Hidaka K, Kimura T, Hayashi Y, Kiso Y, Kuroki R (2009) Structure of HIV-1 protease in complex with potent inhibitor KNI-272 determined by high-resolution X-ray and neutron crystallography. Proc Natl Acad Sci USA 106:4641–4646
64. Suguna K, Padlan EA, Smith CW, Carlson WD, Davies DR (1987) Binding of a reduced peptide inhibitor to the aspartic proteinase from Rhizopus chinensis: implications for a mechanism of action. Proc Natl Acad Sci U S A 84:7009–7013
65. Chong LT, Duan Y, Wang L, Massova I, Kollman PA (1999) Molecular dynamics and free-energy calculations applied to affinity maturation in antibody 48G7. Proc Natl Acad Sci USA 96:14330–14335
66. Knecht V (2010) Model amyloid peptide B18 monomer and dimer studied by replica exchange molecular dynamics simulations. J Phys Chem B 114:12701–12707